SLM-Based System for Localized Targeted Irradiation of Cells and Noninvasive Monitoring of Cell Death

Andrey V. Belashov[1], Anna A. Zhikhoreva[1*], Maxim V. Belashov[1,2], Anna V. Salova[3], Tatiana N. Belyaeva[3], Ilia K. Litvinov[3], Elena S. Kornilova[3], and Irina V. Semenova[1]

[1] Ioffe Institute, Russian Academy of Sciences, 26 Polytekhnicheskaya str., St. Petersburg 194021, Russian Federation
[2] ITMO University, 49 Kronverkskiy pr., St. Petersburg 197101, Russian Federation
[3] Institute of Cytology, Russian Academy of Sciences, 4 Tikhoretsky pr., St. Petersburg 194064, Russian Federation
*e-mail: anna_zhikhoreva@mail.ru

Abstract. The paper presents the development and validation of an experimental technique enabling localized targeted photodynamic treatment at subcellular level and further noninvasive monitoring of variations in cell morphology using low-coherence holographic microscopy realized in the configuration of spatial light interference microscopy (SLIM). The key element of the setup is spatial light modulator (LCOS SLM) which enabled both the targeted irradiation and continuous quantitative monitoring of cell response. To confirm the reconstruction accuracy of phase images of microscopic objects, a test sample comprising a set of polystyrene microspheres was analyzed. Targeted photodynamic treatment was tested by localized irradiation of HeLa cells photosensitized with Radachlorin. Irradiation of cells triggered their death by apoptosis and necrosis. SLIM-assisted monitoring of cells provided quantitative data on the dynamics of changes in their morphological parameters caused by treatment.

Keywords: spatial light interference microscopy (SLIM); spatial light modulator (LCOS SLM); localized irradiation; targeted photodynamic treatment; photosensitizer; Radachlorin; apoptosis; necrosis.

Paper #9486 received 23 Jan 2026; revised manuscript received 15 Apr 2026; accepted for publication 20 Apr 2026; published online 9 June 2026. doi: 10.18287/JBPE26.12.020307.

1 Introduction

Spatial light modulators (SLMs) enabling arbitrary changes of the amplitude and phase distributions in the light field with a response time of several milliseconds [1] have found wide application in various fields of modern physics [2]. The applications include data transmission [3], information encoding and decoding [4], monitoring of microscopic objects [5], improvement of microscopic techniques [6], etc. An important area of application of these devices is development of optical methods related to phase imaging [7, 8], generation of optical beams with specific properties [9], or creation of augmented reality (AR) displays [10]. Utilization of Liquid Crystal on Silicon Spatial Light Modulators (LCOS SLM) for recording phase images of various biological objects has been repeatedly demonstrated, see e.g. [11–13]. The ability of these devices to precisely control the phase distribution of the wavefront allows generating arbitrary intensity distributions on the sample, which was applied for creation of optical tweezers [14], focusing laser radiation through scattering tissues [15, 16], and local action on different areas of a sample in optogenetics [17].

Photodynamic therapy (PDT) is a promising cancer treatment modality, which enables intracellular generation of reactive oxygen species (ROS) upon light irradiation of photosensitizer (PS) molecules. As known, the PDT efficacy and initiation of specific cell death pathways depend on intracellular distribution and localization of PS molecules [18, 19]. The subcellular organelle-targeted treatment strategies providing an impact directed precisely onto specific organelles receive growing research interest as a promising cancer treatment modality, however specific details of cell death processes still remain poorly understood [20]. Several PSs have been developed that selectively accumulate in specific organelles, including plasma membrane, nuclei, mitochondria, lysosomes,

This paper was presented at the International Russian-Chinese Workshop on Light for Life Sciences, St. Petersburg, Russian Federation, October 17 – 20, 2025.

endoplasmic reticulum and Golgi apparatus (see Ref. [21] and references therein). Further localized irradiation of the photosensitized organelles causes localized generation of ROS and allows for investigation of cellular response to damage of these compartments, which can help understand their functioning, assess intercellular signaling associated with cell death and cell resistance to treatment and oxidative stress [22]. Less selective targeted irradiation of individual photosensitized cells or groups of cells in a sample with different irradiation durations can be used to analyze cell resistance to different treatment doses [23].

The response of cells to photodynamic treatment of specific organelles requires long-term noninvasive monitoring of the samples. The techniques of quantitative phase imaging (QPI), being label-free and utilizing low-power radiation, are best suited for assessing quantitative data on variations of morphological and optical parameters of cells in dynamics [23–25]. One of the promising QPI techniques is spatial light interference microscopy (SLIM) [13], which can be realized on common biological microscopes and allows for combination with fluorescence-based measurements in a single multimodal system [7].

In this paper, we present the developed experimental approach enabling localized targeted irradiation at subcellular level and further noninvasive monitoring of variations in cell morphology using SLIM. The technical realization of the approach was based on utilization of a spatial light modulator, which allowed for both the targeted irradiation and continuous quantitative monitoring of cell response. The approach was validated on localized photodynamic treatment of HeLa cells photosensitized with Radachlorin PS.

2 Methods and Materials

2.1 Spatial Light Interference Microscopy

The low-coherence quantitative phase imaging in the SLIM configuration was implemented on an inverted fluorescence microscope Nikon Ti-2A using the LCOS SLM PLUTO-2.1 NIR-133 (Holoeye) by creating an external channel of phase-contrast imaging. The phase shift of the reference wave, not scattered in the course of its propagation through the object, was formed on the SLM located in the plane conjugate to the image plane, as shown in Fig. 1(a). A ring-shaped phase pattern, mimicking the annular aperture of sample illumination, was formed on the SLM and phase shifts were sequentially introduced into the reference wave in the range of 0–3π/2 with the π/2 step, as illustrated in the inset in Fig. 1(a). This enabled observation of phase-contrast images of cytological samples without utilization of special phase-contrast microobjectives. In experiments, we used a 40× microobjective with numerical aperture of 1.15 and working distance of 0.6 mm.

For radiation source in the SLIM setup we used the standard LED light source of the Nikon microscope, the working range of 510–560 nm was selected by a bandpass filter BP535/50 (Chroma). The reference wave reflected from the phase-shifting ring on the SLM interfered with the object wave, scattered by the sample and passed by the phase-shifting ring, on the sensor matrix of the digital camera ToupCam UHCCD05000KPA (Touptek, China). The phase distribution of the object wave was then reconstructed from the four recorded phase-shifted holograms using a phase-step algorithm [26], modified for proper account of a partial contribution of light scattered by the sample into the reference wave (annular aperture) [27, 28]. Propagation of a fraction of light scattered by the sample through the ring aperture of the reference wave may lead to formation of halo-shaped image artifacts, which should then be eliminated using a filtering procedure [29, 30]. A more detailed description of the data processing algorithms used for data retrieval in the SLIM technique can be found in Ref. [13].

Despite the artifacts associated with the incomplete separation of the reference and object waves, utilization of low-coherence radiation for hologram recording enables elimination of coherent noise [31, 32], which is a source of a reduced image quality in traditional off-axis digital holographic microscopy based on the Mach-Zehnder interferometer and utilizing laser as a radiation source (Fig. 1(b)). The lack of coherent noise in SLIM allows increasing the spatial resolution and phase-shift measurement accuracy on the obtained images. Besides that, implementation of this approach on a standard inverted microscope enables combination of this technique with other methods, fluorescence analysis in particular [7].

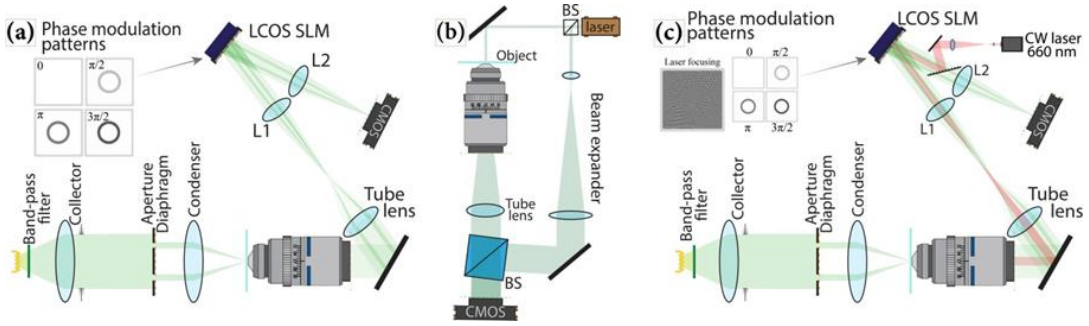

Fig. 1 Schematics of the experimental setups: (a) spatial light interference microscopy, (b) off-axis digital holographic microscopy, (c) spatial light interference microscopy with localized irradiation of a sample.

2.2 Localized Photodynamic Treatment of Individual Cells

As known, along with implementation of the external phase contrast with controlled phase distribution LCOS SLMs can also be used to generate laser beams with specific properties [33, 34], or to shape arbitrary intensity distributions in a desired plane by generating a specific phase pattern and then diffracting the resulting wavefront [35, 36]. The quite short response time of the SLMs (10.5 ms for PLUTO-2.1) enables a multipurpose utilization of this device in the course of a single experiment. In our realization the modulator was used for both localized targeted laser irradiation of individual photosensitized cells and subsequent monitoring of changes in their morphology in the SLIM channel. The experimental schematic is illustrated in Fig. 1(c).

Experiments were performed on samples of live cells of the established line HeLa (human cervix epidermoid carcinoma). Cell samples were obtained from the shared research facility "Vertebrate Cell Culture Collection" of the Institute of Cytology RAS. Cells were grown in monolayers in Petri dishes at 37 ℃ in 5% CO_2 atmosphere for 48 h in the Dulbecco modified Eagle medium (DMEM) (GIBCO, USA) supplemented with 10% fetal bovine serum (FBS) (GIBCO, USA) and 1% penicillin-streptomycin. After that Radachlorin photosensitizer (RadaPharma) was added to the culture medium at the concentration of 20 μg/ml, and cells were incubated in this solution for 24 h. Our previous work [37] has shown that 24-h incubation with Radachlorin provides efficient uptake of PS molecules by cells and their accumulation mostly in cellular lysosomes. After that, the cells were washed in PBS and fresh culture medium was added to the sample. For photodynamic treatment several cells in the sample were exposed to laser radiation at 660 nm, at the maximum of Q absorption band of the PS. Irradiation caused excitation of PS molecules in cells and induced generation of reactive oxygen species, triggering cell death.

It is worth noting that accumulated photosensitizer caused enhanced photosensitivity of cells in the wavelength range corresponding to the absorption spectrum of the PS, therefore the wavelength range of light used for monitoring the cytological sample in the SLIM setup should be outside the absorption band of the PS. Radachlorin absorption in the ranges of 300–450 nm and 590–690 nm limits utilization of blue and red light for cells' monitoring. The working spectral range of our setup of 510–530 nm allowed for noninvasive monitoring of cells for extended periods of time.

3 Results

3.1 Validation of the SLIM Performance

The operability of the experimental setup and performance of algorithms developed for processing of four on-axis interference patterns and retrieval of the resulting phase distributions have been validated using a test microscopic object comprising polystyrene beads, 2 μm in diameter ($n = 1.593$) placed in glycerol ($n = 1.477$) (Fig. 2). Differential interference contrast (DIC) images of beads are shown in Fig. 2(a).

The known parameters of the beads and surrounding medium allowed us to simulate phase distributions introduced by these microspheres into the transmitted wavefront and to compare them with the experimentally obtained phase distributions. Note that according to the manufacturer, the bead diameter could deviate from 2 μm in 10–15%. To conduct the validation experiment the microsphere concentration was chosen to minimize aggregation and prevent formation of multi-layer structures, which would complicate numerical processing of the resulting phase-shift patterns. Phase images of the beads were recorded in the SLIM channel (Fig. 2(b)).

For additional verification of the results obtained we also recorded off-axis digital holograms of the same test object by means of the traditional coherent holographic microscopy, which allowed us to eliminate the first-order diffraction and to reconstruct the corresponding spatial distributions of phase shift using Fourier transform (Fig. 2(c)). Comparison of the simulated phase distributions with those obtained experimentally using low-coherence SLIM and off-axis digital holography with coherent laser radiation (Fig. 2(d)) demonstrated that low-coherence phase imaging provides reliable data on phase shift distributions of phase objects.

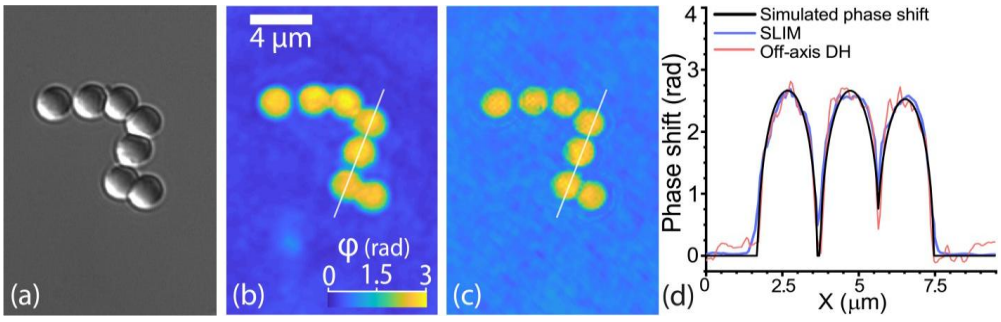

Fig. 2 Images of beads obtained by: (a) DIC, (b) SLIM, (c) off-axis holographic microscopy with the coherent light source. (d) Comparison of the simulated phase distribution with those obtained from images in panels (b) and (c) for the three beads marked by the white line.

The measurement error in SLIM did not exceed 0.05 radians. This error was due to a combination of various factors, such as defects in the bead shape, the accuracy of phase pattern formation on the SLM, halo-related data processing artifacts, noise on the photodetector during image acquisition, potential microscopic movement of the object during image acquisition, etc. The halo filtering was performed using the algorithm described in Ref. [29].

3.2 Analysis of the Response of Individual Cells to Localized Photodynamic Treatment

To generate the desired arbitrary pattern of localized laser irradiation of cells, we first recorded an image of a group of cells using wide-field microscopy. The local areas chosen to be subjected to laser irradiation were marked on this image (Fig. 3(a)). According to our previous work [37], Radachlorin accumulates mainly in lysosomes; in HeLa cells these organelles are clustered in the perinuclear area. Therefore, radiation was focused onto the presumed locations of lysosome clusters. These locations were selected by visual observation of maximal intensity of Radachlorin fluorescence in the perinuclear areas using the microscope camera. The areas subjected to irradiation at 660 nm are indicated in Fig. 3(a) by yellow arrows.Then the phase pattern was calculated, so that diffraction of laser radiation would lead to formation of the required intensity distribution on the sample [38, 39]. Subsequent observation of the combined image of the cells and the formed pattern of localized laser irradiation allowed us to adjust the generated pattern and make corrections to spot locations or sizes, if necessary. Note that the minimal diameter of the irradiation spot in our setup was about 0.7 μm, which allows for selective targeted irradiation of larger cellular compartments, such as nucleus, Golgi apparatus, lysosomal clusters and endoplasmic reticulum. The technique also allows regulating the relative intensity of laser irradiation in different areas of the field of view; however, in this study the initial laser radiation power was distributed uniformly among all irradiated locations in cells (≈ 2.6 μW at each spot).

Irradiation of the chosen areas in photosensitized cells for 5 min led to excitation of photosensitizer molecules and intracellular generation of reactive oxygen species, which initiated cell death. After irradiation of cells, the SLM was reconfigured for operation in the SLIM setup and a set of digital holograms of the field of view was recorded aimed for monitoring the cell response to treatment. Examples of the phase images of the group of cells shown in Fig. 3(a) obtained in the course of their post-treatment monitoring are demonstrated in Fig. 3(c). As can be seen in Fig. 3(c), localized photodynamic treatment of three of six HeLa cells in the group (cells 4, 5, 6), caused variations, characteristic of death processes.

Significant changes in morphology of the cells 5 and 6 (initial formation of small bubbles and subsequent membrane damage and efflux of the intracellular medium manifested by formation of large bubbles) are clearly visible on the phase images in Fig. 3(c). Such changes are characteristic of cell necrosis. At the same time, the cell 4 shows a different scenario of changes (initial formation of small bubbles and, after some time, an increase in the phase shift), characteristic for cell apoptosis. Phase images of non-irradiated cells (cells 1, 2, 3) clearly demonstrate the absence of any changes in cell morphology, validating their survival.

We have previously shown that the value of phase shift, averaged over the entire cell, is a robust quantitative parameter, characterizing death-specific variations in cellular morphology [24]:

$$\varphi_{av} = \frac{1}{S_{cell}} \int_{S_{cell}} \Delta\varphi(x,y)dxdy, \qquad (1)$$

where $Q = 2.26 \cdot 10^6$ J/kg – specific heat of water where $\Delta\varphi(x, y)$ is the phase shift introduced by a cell to the transmitted wave front in a certain point (x, y) and S_{cell} is the cell projected area.

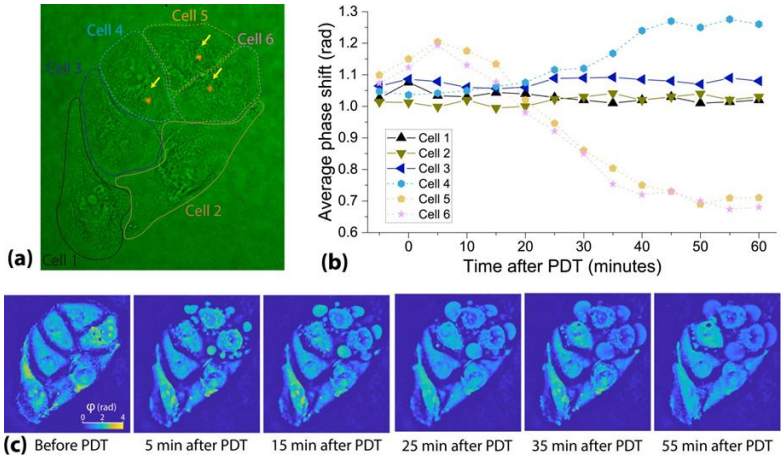

Fig. 3 (a) Bright-field microscopic image of 6 HeLa cells, yellow arrows indicate the areas of localized irradiation. (b) Average phase shift in 6 HeLa cells before and after localized irradiation of the three cells (cells 4, 5, 6). (c) Phase images of the same HeLa cells before and after PDT.

The dynamics of average phase shift after photodynamic treatment was shown in Ref. [24] to clearly correlate with the type of cell death. Utilization of the commonly used fluorescent live-dead test assays, Acridine Orange and Ethidium Bromide (AO/EB) and Annexin V/Propidium Iodide, allowed us to validate that an exponential decrease of the average phase shift was characteristic of cell necrosis, while its increase was due to cell dehydration and rounding in the course of apoptosis. The absence of average phase shift variations at low irradiation doses corresponded to cell survival, which was also confirmed by the fluorescence test assays. These results provided a basis for drawing conclusions on death pathways of cells from the dynamics of average phase shift in individual cells observed in this study. Note that this method is noninvasive and does not require utilization of additional exogenous fluorescent dyes. Mention that spatial distribution of the parameter $\Delta\varphi(x, y)$ can also be used further for calculation of several important morphological and physiological parameters of cells [40], for analysis of cell states [23, 41] and rates of their death [42].

Figure 3(b) shows the dynamics of average phase shift in all the six cells shown in Fig. 3(a). As can be seen from the graphs, the dynamics of φav in non-irradiated cells clearly demonstrate the absence of statistically significant variations of this parameter, while that in the cell 4 is characteristic for apoptosis and those in cells 5 and 6 – for secondary necrosis (see Ref. [24] for the detailed explanation).

It is worth noting that, despite the same irradiation doses applied to the three cells, one of them (cell 4) underwent apoptosis, while two others (cells 5 and 6) died by necrosis. This may be due to both a lower amount of photosensitizer in the irradiated area of cell 4 and to the higher resistance of this cell to photodynamic treatment, which could be due to such factors as, e.g., different phase of the cell cycle or lower amount of oxygen in the area subjected to treatment. The heterogeneity in cell response to photodynamic treatment at the same dose and within the single sample was also demonstrated in our recent paper [41]. It was shown that at each irradiation dose in the sample there were cells in all the three states: live, apoptotic and necrotic. However, depending upon the dose one of the states prevailed.

4 Summary and Conclusions

Therefore, we implemented and tested the experimental setup based on the inverted fluorescence microscope and LCOS SLM for localized photodynamic treatment and noninvasive monitoring of living cells. Validation of the performance of SLIM channel on the model object providing the phase shift similar to that of living cells in a culture medium demonstrated that this low-coherence QPI method enables reconstruction of high-quality phase images of microscopic objects. The spatial light modulator used to generate interference patterns with a specified phase shift was shown to be applicable also for localized irradiation of cells. Its operationability was demonstrated on targeted photodynamic treatment of HeLa cells photo- sensitized with Radachlorin. The small size of the irradiation spot enables selective targeted irradiation of individual cellular compartments, such as nucleus, Golgi apparatus, lysosomal clusters and endoplasmic reticulum. The appropriate selection of the spectral range for QPI allows for long-term noninvasive monitoring of photosensitized cells without significant changes in their morphological or physiological parameters. We have shown that utilization of the LCOS SLM allows implementation of a full range of experimental methods for studying the mechanisms of photodynamic treatment of individual cells. Although studies of cell response to external stimuli are typically conducted on a large population of cells to obtain statistically significant results, the sub-cellular targeted localized treatment and further noninvasive monitoring of individual cells may be quite promising for more deep analysis of subtle intracellular processes in response to specific treatment modalities.

Declaration of Competing Interests

The authors declare that they have no known competing financial interests or personal relationships that could have appeared to influence the work reported in this paper.

Data Availability

Data will be made available on request.

References

1. M. Pivnenko, K. Li, and D. Chu, "Sub-millisecond switching of multi-level liquid crystal on silicon spatial light modulators for increased information bandwidth," Optics Express 29(16), 24614–24628 (2021).
2. Y. Yang, A. Forbes, and L. Cao, "A review of liquid crystal spatial light modulators: devices and applications," Opto-Electronic Science 2(8), 230026 (2023).
3. M. Wang, L. Zong, L. Mao, A. Marquez, Y. Ye, H. Zhao, and F. Vaquero Caballero, "LCoS SLM study and its application in wavelength selective switch," Photonics 4(2), 22 (2017).
4. T. Z. Minikhanov, E. Y. Zlokazov, P. A. Cheremkhin, R. S. Starikov, and N. N. Evtikhiev, "Computer-generated holography methods for data page reconstruction using phase-only medium," Applied Sciences 13(7), 4479 (2023).
5. Y. Lin, H.-C. Chen, H.-Y. Tu, C.-Y. Liu, and C.-J. Cheng, "Optically driven full-angle sample rotation for tomographic imaging in digital holographic microscopy," Optics Letters 42(7), 1321 (2017).

6. C. Garbellotto, J. M. Taylor, "Multi-purpose SLM-light-sheet microscope," Biomedical Optics Express 9(11), 5419 (2018).
7. A. A. Zhikhoreva, A. V. Belashov, A. V. Salova, I. K. Litvinov, T. N. Belyaeva, E. S. Kornilova, I. V. Semenova, and O. S. Vasyutinskii, "QPI- and FLIM-assisted multimodal analysis of the dynamics of morphological and physiological parameters of cells," Light: Advanced Manufacturing 6(4), 843–855 (2026).
8. J. Chatterjee, K. Bhattacharya, "High resolution microscopic imaging using a phase SLM," Journal of Optics 54(2), 286–291 (2025).
9. A. Keskin, G. Kaya, N. Kaya, J. Strohaber, A. A. Kolomenskii, and H. A. Schuessler, "Dynamic control of airy beams using real-time phase-amplitude encoding on a spatial light modulator," Optics 5(4), 581–594 (2024).
10. K. Fan-Chiang, S. Huang, C. Shen, H. Wang, Y. Li, H. Tsai, and Y. Huang, "Analog LCOS SLM devices for AR display applications," Journal of the Society for Information Display 28(7), 581–590 (2020).
11. C. Fan, H. Zhao, Z. Zhao, J. Li, Y. Du, X. Yang, and L. Zhang, "Single-shot quantitative phase imaging with phase modulation of a liquid crystal spatial light modulator (LC-SLM) under white light illumination," Optics Letters 47(20), 5264 (2022).
12. I. Shevkunov, V. Katkovnik, N. V. Petrov, and K. Egiazarian, "Super-resolution microscopy for biological specimens: lensless phase retrieval in noisy conditions," Biomedical Optics Express 9(11), 5511 (2018).
13. Z. Wang, L. Millet, M. Mir, H. Ding, S. Unarunotai, J. Rogers, M. U. Gillette, and G. Popescu, "Spatial light interference microscopy (SLIM)," Optics Express 19(2), 1016 (2011).
14. I. A. Favre-Bulle, A. B. Stilgoe, E. K. Scott, and H. Rubinsztein-Dunlop, "Optical trapping *in vivo*: theory, practice, and applications," Nanophotonics 8(6), 1023–1040 (2018).
15. I. Galaktionov, A. Nikitin, J. Sheldakova, V. Toporovsky, and A. Kudryashov, "Focusing of a laser beam passed through a moderately scattering medium using phase-only spatial light modulator," Photonics 9(5), 296 (2022).
16. S. Mukherjee, A. Vijayakumar, and J. Rosen, "Spatial light modulator aided noninvasive imaging through scattering layers," Scientific Reports 9(1), 17670 (2019).
17. Z. Zhang, L. E. Russell, A. M. Packer, O. M. Gauld, and M. Häusser, "Closed-loop all-optical interrogation of neural circuits *in vivo*," Nature Methods 15(12), 1037–1040 (2018).
18. F. M. Engelmann, I. Mayer, D. S. Gabrielli, H. E. Toma, A. J. Kowaltowski, K. Araki, and M. S. Baptista, "Interaction of cationic meso-porphyrins with liposomes, mitochondria and erythrocytes," Journal of Bioenergetics and Biomembranes 39(2), 175–185 (2007).
19. B. W. Pogue, B. Ortel, N. Chen, R. W. Redmond, and T. Hasan, "A photobiological and photophysical-based study of photo- toxicity of two chlorins," Cancer Research 61(2), 717–724 (2001).
20. J. Yang, A. Griffin, Z. Qiang, and J. Ren, "Organelle-targeted therapies: a comprehensive review on system design for enabling precision oncology," Signal Transduction and Targeted Therapy 7(1), 379 (2022).
21. X. Du, S. Huang, Z. Lin, G. Chen, Y. Jiang, and H. Zhang, "Organelle-targeted small molecular photosensitizers for enhanced photodynamic therapy: a minireview for recent advances and potential applications," Chemical Communications 61(40), 7236–7252 (2025).
22. M. J. Iqbal, A. Kabeer, Z. Abbas, H. A. Siddiqui, D. Calina, J. Sharifi-Rad, and W. C. Cho, "Interplay of oxidative stress, cellular communication and signaling pathways in cancer," Cell Communication and Signalling 22(1), 7 (2024).
23. A. V. Belashov, A. A. Zhikhoreva, A. V. Salova, T. N. Belyaeva, I. K. Litvinov, E. S. Kornilova, and I. V. Semenova, "SLIM-assisted automatic cartography of cell death types and rates resulting from localized photodynamic treatment," Journal of the Optical Society of America A 41(11), C72 (2024).
24. A. V. Belashov, A. A. Zhikhoreva, T. N. Belyaeva, N. N. Nikolsky, I. V. Semenova, E. S. Kornilova, and O. S. Vasyutinskii, "Quantitative assessment of changes in cellular morphology at photodynamic treatment in vitro by means of digital holographic microscopy," Biomedical Optics Express 10(10), 4975 (2019).
25. A. V. Belashov, A. A. Zhikhoreva, V. G. Bespalov, V. I. Novik, N. T. Zhilinskaya, I. V. Semenova, and O. S. Vasyutinskii, "Refractive index distributions in dehydrated cells of human oral cavity epithelium," Journal of the Optical Society of America B 34(12), 2538 (2017).
26. I. Shevkunov, N. V. Petrov, "Phase retardation analysis in a rotated plane-parallel plate for phase-shifting digital holography," Journal of Imaging 8(4), 87 (2022).
27. Z. Wang, G. Popescu, "Quantitative phase imaging with broadband fields," Applied Physics Letters 96(5), 051117 (2010).
28. G. Popescu, L. P. Deflores, J. C. Vaughan, K. Badizadegan, H. Iwai, R. R. Dasari, and M. S. Feld, "Fourier phase microscopy for investigation of biological structures and dynamics," Optics Letters 29(21), 2503–2505 (2004).
29. Y. Pan, S. Guo, Z. J. Smith, and K. Chu, "Simultaneous 3D deconvolution and halo removal for spatial light interference microscopy through a two-edge apodized Wiener filter," Journal of the Optical Society of America A 39(2), 287–296 (2022).
30. T. H. Nguyen, M. Kandel, H. M. Shakir, C. Best-Popescu, J. Arikkath, M. N. Do, and G. Popescu, "Halo-free phase contrast microscopy," Scientific Reports 7(1), 44034 (2017).

31. A. A. Kerov, A. V. Kozlov, P. A. Cheremkhin, A. V. Shifrina, R. S. Starikov, E. Y. Zlokazov, E. K. Petrova, V. A. Nebavskiy, and N. N. Evtikhiev, "Speckle noise reduction in digital holography by 3D adaptive filtering," Sensors 25(17), 5402 (2025).
32. P. A. Cheremkhin, N. N. Evtikhiev, A. V. Kozlov, V. V. Krasnov, V. G. Rodin, and R. S. Starikov, "An optical-digital method of noise suppression in digital holography," Journal of Optics 24(11), 115702 (2022).
33. R. Bowman, N. Muller, X. Zambrana-Puyalto, O. Jedrkiewicz, P. Di Trapani, and M. J. Padgett, "Efficient generation of Bessel beam arrays by means of an SLM," The European Physical Journal Special Topics 199(1), 159–166 (2011).
34. C. Rosales-Guzmán, N. Bhebhe, and A. Forbes, "Simultaneous generation of multiple vector beams on a single SLM," Optics express 25(21), 25697 (2017).
35. V. Nikolenko, D. S. Peterka, R. Araya, A. Woodruff, and R. Yuste, "Spatial light modulator microscopy," Cold Spring Harbor Protocols 2013(12), pdb.top079517 (2013).
36. X. Li, Y. Zhou, Y. Cai, Y. Zhang, S. Yan, M. Li, R. Li, and B. Yao, "Generation of hybrid optical trap array by holographic optical tweezers," Frontiers in Physics 9, 591747 (2021).
37. A. V. Belashov, A. A. Zhikhoreva, A. V. Salova, T. N. Belyaeva, I. K. Litvinov, E. S. Kornilova, I. V. Semenova, and O. S. Vasyutinskii, "Analysis of Radachlorin localization in living cells by fluorescence lifetime imaging microscopy," Journal of Photochemistry and Photobiology B: Biology 243, 112699 (2023).
38. Y. Wu, J. Wang, C. Chen, C.-J. Liu, F.-M. Jin, and N. Chen, "Adaptive weighted Gerchberg-Saxton algorithm for generation of phase-only hologram with artifacts suppression," Optics Express 29(2), 1412–1427 (2021).
39. D. Kim, A. Keesling, A. Omran, H. Levine, H. Bernien, M. Greiner, M. D. Lukin, and D. R. Englund, "Large-scale uniform optical focus array generation with a phase spatial light modulator," Optics Letters 44(12), 3178 (2019).
40. P. Girshovitz, N. T. Shaked, "Generalized cell morphological parameters based on interferometric phase microscopy and their application to cell life cycle characterization," Biomedical Optics Express 3(8), 1757 (2012).
41. A. V. Belashov, A. A. Zhikhoreva, T. N. Belyaeva, A. V. Salova, E. S. Kornilova, I. V. Semenova, and O. S. Vasyutinskii, "Machine learning assisted classification of cell lines and cell states on quantitative phase images," Cells 10(10), 2587 (2021).
42. A. A. Zhikhoreva, A. V. Belashov, A. B. Danilova, N. A. Avdonkina, I. A. Baldueva, M. L. Gelfond, T. L. Nekhaeva, I. V. Semenova, and O. S. Vasyutinskii, "Significant difference in response of malignant tumor cells of individual patients to photodynamic treatment as revealed by digital holographic microscopy," Journal of Photochemistry and Photobiology B: Biology 221, 112235 (2021).